eprints@whiterose.ac.uk
https://eprints.whiterose.ac.uk/

RSC Advances

ARTICLE

One-pot synthesis and characterization of reduced graphene oxide–gelatin nanocomposite hydrogels

Yongzhe Piao and Biqiong Chen*

Reduced graphene oxide (RGO)-gelatin nanocomposite hydrogels were prepared via a facile one-pot synthesis by heating the mixture of an aqueous graphene oxide (GO) suspension and a gelatin solution at the desired ratio at 95 °C for 24 h. The hydrogels were formed mainly by chemically cross-linking gelatin macromolecular chains with graphene nanosheets where gelatin acts as a reducing agent to convert GO to RGO and chemically grafted onto the graphene surface. Fourier transform infrared spectroscopy, Raman spectroscopy, X-ray diffraction and scanning electron microscopy were employed to characterize the RGO-gelatin nanocomposite hydrogels. Rheological tests showed that the storage modulus of the hydrogels was up to 172.3 kPa. Water swelling tests found that the swelling behavior of the dried hydrogels followed Fick's diffusion law, with an equilibrium swelling ratio of up to 44.7. The enzymatic degradation tests demonstrated that the hydrogels lost up to 29% of their original weight after degradation for 24 h. The relatively high mechanical properties and biodegradability could provide RGO-gelatin hydrogels potential in tissue engineering and drug delivery.

Introduction

Hydrogels are three-dimensional networks of cross-linked hydrophilic polymers that contain a high amount of water without dissolving. They have been extensively studied for applications such as tissue engineering, drug delivery, biosensing, and superabsorption in the hygienic and agriculture area.[1, 2] The soft and wet characteristics of hydrogels closely resemble biological tissues, making them attractive candidates for biomedical applications.[3] However, the drawbacks of conventional hydrogels, such as poor mechanical properties and toxicity of organic cross-linking agents,[4, 5] restrict their applications.

To overcome some of the drawbacks, polymer nanocomposite hydrogels have recently attracted significant attention from researchers. Haraguchi and Takehisa[6] reported a poly(N-isopropyl acrylamide)-hectorite nanocomposite hydrogels with a tensile strength of 109 kPa at a water content of 88 wt.%. Recently, Hu and Chen[7] reported polyacrylamide (PAM)-layered double hydroxide nanocomposite hydrogels showing a storage modulus of about 220 Pa at a water content of 94 wt.%.

Graphene is a flexible one-atom thick, two-dimensional (2D) carbon sheet with a honeycomb structure.[8] Because of its exceptional properties, including high electron mobility, mechanical properties and surface area, graphene has recently attracted tremendous attention in various applications, such as optoelectronics, energy storage, catalysis, gas sensing, super-capacitors, thermoelectric devices, composites, tissue engineering and drug delivery.[8-14] A practical and scalable approach to produce graphene is chemical reduction of graphene oxide (GO).[15] This product is known as reduced graphene oxide (RGO) or chemically converted graphene,[16] which inherits most interesting properties of graphene. Graphene is non-toxic at low concentrations,[17, 18] and its toxicity could be further reduced by surface functionalization with a biocompatible polymer.[19, 20] According to *in vitro* and/or *in vivo* animal experiments,[21, 22] biocompatible poly(ethylene glycol) (PEG)-functionalized graphene nanosheets show excellent biocompatibility and can be excreted from the body by metabolism after intravenous and intraperitoneal administration.

RGO-based hydrogels have been investigated for applications in energy storage, electronics, electrochemistry and healthcare.[23-26] A self-assembled RGO hydrogel was first reported by Xu and co-workers[24] in 2010, showing high specific capacitances. In this work, GO sheets were reduced to RGO sheets through a hydrothermal process and self-assembled to a hydrogel via π-π stacking. Since then, a number of graphene-inorganic composite hydrogels, such as graphene-Ni(OH)$_2$ composite hydrogels[25] and graphene-VO$_2$ nanobelt composite hydrogels,[26] were developed, which exhibited further improved capacitances.

Graphene-polymer nanocomposite hydrogels have also been investigated. Graphene-PAM hydrogels were synthesized via *in situ* polymerization of acrylamide in an aqueous suspension of PAM-stabilized graphene, showing a compressive strength of 9 kPa and a storage modulus of 7 kPa at a water content of about 90 wt.%.[27] At a similar water content, RGO-poly(N,N-dimethylacryl-amide) (PDMAA) hydrogels were synthesized as potential tissue scaffolds by *in situ* polymerization of DMAA within a pre-formed graphene hydrogel, giving a high compressive strength of 2.62 MPa due to their dual network structures.[28] A graphene-poly(3,4-ethylenedioxythiophene) (PEDOT) hydrogel exhibited a compressive strength of 29.6 MPa and a storage modulus of 2.1 MPa at a water

Department of Materials Science and Engineering, University of Sheffield, Mappin Street, Sheffield S1 3JD, United Kingdom, E-mail: biqiong.chen@sheffield.ac.uk; Fax: +44 (0) 114 222 5943; Tel: +44 (0) 114 222 5958

content of 59.5 wt.% mainly because of the high solid content and the strong physical interaction between PEDOT chain and graphene.[29] These nanocomposite hydrogels were synthesized by in *situ* polymerization in which the monomer was polymerized in the presence of graphene nanosheets. Self-assembly method was also employed to synthesize RGO-polymer nanocomposite hydrogels. For example, RGO-containing dipeptide hydrogels were synthesized and showed a storage modulus of 41 kPa at a water content of 99.5 wt.%.[30] A RGO-agarose hydrogel was fabricated for miniature-scale water purification.[31]

Gelatin is a denatured biopolymer, derived from collagen, with abundant amino groups on its molecular chains.[32] It possesses distinctive characteristics, such as biocompatibility, remarkable affinity to proteins, biodegradability and low cost, therefore it is commonly used for pharmaceutical and medical applications.[33] Gelatin has been used in hydrogel developments for drug delivery, tissue engineering, gene therapy and biosensing.[32] Self-assembled graphene oxide-gelatin nanocomposite hydrogels were previously reported by our group, which exhibited a storage modulus of 54.0–114.5 kPa with 98.0–98.5 wt.% water.[34] GO-poly(acrylic acid)-gelatin nanocomposite hydrogels were reported by others, which presented a tensile strength of 150–250 kPa with ~90 wt.% water,[35] and a compressive strength of 7–26 MPa with 29–51 wt.% water content,[36] mainly owing to their strong semi-interpenetrating network comprising chemically cross-linked poly(acrylic acid) and loose gelatin chains as well as the low water contents. UV cross-linked GO-gelatin methacrylate composite hydrogels were also reported, which showed a compressive strength of 91.3–976.7 kPa at a water content of 94.3–94.5 wt.%.[37] Furthermore, gelatin functionalized graphene nanosheets were prepared for drug delivery and cellular imaging, in which gelatin chains reduced GO and grafted onto the surface of the resultant RGO nanosheets,[20] In this case, gelatin not only improved biocompatibility of graphene nanosheets, but also acted as a reducing agent to reduce GO to RGO under mild heating forming covalent bonding with RGO through its amino groups. These findings indicate the possibility of creating strong RGO-gelatin nanocomposite hydrogels based on GO and gelatin.

Inspired by the above concept, novel RGO-gelatin hydrogels were synthesized by a green and facile method in the current work, i.e., one-pot synthesis of multiply cross-linked hydrogels via a mild heating process, without using any chemical cross-linkers or organic solvents. GO and gelatin were used as the starting materials to prepare the nanocomposite hydrogel. We hypothesized that chemical cross-linking would be built between gelatin chains and graphene nanosheets to form a robust 3D network in which GO was reduced to RGO by gelatin during the mild heating process. The absence of a toxic chemical makes this approach attractive for some biomedical applications. The structure, rheological properties, swelling behavior and biodegradation of the nanocomposite hydrogels were investigated in detail.

Experimental

Materials

Graphite powder (size < 20 μm), gelatin (type B, BioReagent, bloom strength 225, number average molecular weight: 50,000),

collagenase type II from Clostridium histolyticum (≥ 125 CDU mg^{-1} solid), Dulbecco's phosphate buffered saline (PBS, with MgCl$_2$ and CaCl$_2$, pH = 7.4), potassium permanganate (KMnO$_4$), sodium nitrate (NaNO$_3$), hydrogen peroxide (H$_2$O$_2$, 30%), concentrated sulphuric acid (H$_2$SO$_4$, 98%), and hydrochloric acid (HCl, 35%) were all purchased from Sigma-Aldrich and used as received.

Preparation of RGO-gelatin nanocomposite hydrogels

GO was synthesized from graphite powder using a modified Hummers' method,[38, 39] purified and freeze-dried.[34] RGO-gelatin nanocomposite hydrogels were prepared by heating mixtures of a GO aqueous suspension and a gelatin solution with desired ratios at 95 °C for 24 h. The required amount of GO powder was dispersed in distilled water in a glass vial and stirred for 2 h using a magnetic stirrer before it was subjected to 30 min sonication to obtain a fully exfoliated GO suspension. The gelatin solution was prepared by heating a desired amount of gelatin in distilled water at 60 °C for 1 h. In a typical preparation, 0.5 mL gelatin solution (24 mg mL^{-1}) was added into 5.5 mL GO suspension (10.9 mg mL^{-1}) by drop wise while stirring. Then, the mixture, sealed in the glass vial, was heated in an oil bath at 95 °C for 24 h. In this study, a series of RGO-gelatin hydrogels at different material ratios were synthesized. The precursor of the RGO-gelatin hydrogels was the mixture of GO dispersion and gelatin solution comprising of 10 mg mL^{-1} GO, and various concentrations of gelatin, i.e., 2, 5 and 10 mg mL^{-1}, respectively. The RGO-gelatin nanocomposite hydrogels were designated as RGGnH, where n defined the concentration of gelatin in the hydrogels with a unit of mg mL^{-1}.

Characterization

Fourier transform infrared spectroscopy (FT-IR) was carried out on a Perkin Elmer Spectrum 100 Spectrometer, with a resolution of 4 cm^{-1}. Raman spectroscopy was conducted on a Renishaw inVia Raman Spectroscope with 514 nm laser excitation operating at 1 mW. X-ray diffraction (XRD) was achieved with a STOE STADI P X-ray diffractometer with Cu Kα$_1$ radiation (λ = 0.15406 nm) at 40 kV and 35 mA. Diffraction patterns were recorded at a scan speed of 0.27 $^{\circ}$ s^{-1} and with a step size of 0.03° (2θ). Scanning electron microscopy (SEM) was carried out using a FEI Inspect F scanning electron microscope at 10 kV. An aqueous GO suspension (10 mg mL^{-1}), was prepared as described in the preparation section, and RGO-gelatin hydrogels were first frozen in liquid nitrogen, and then dried under vacuum at -10 °C for two days and at room temperature for 30 min in a freeze dryer (FreeZone Triad Freeze Dry System, Labcoco Corporation). The lyophilized sponge-like samples were fractured carefully and fixed on aluminium stubs. All samples were coated with gold using a sputter coater (Emscope SC500A) before the fracture surfaces were observed under SEM. The average pore sizes were calculated by measuring the size of the pores (30 pores) with an ImageJ software.

Atomic force microscopy (AFM) was performed by using a Veeco Instruments Dimension 3100 atomic force microscope operated in tapping mode. A diluted RGO aqueous suspension was dropped onto a freshly cleaved mica surface and left

overnight to dry in air. UV-Vis spectroscopy was performed on a UV/VIS/NIR Spectrometer (Lambda 900, Perkin Elmer), with a scan interval of 1 nm. Thermogravimetric analysis (TGA) was performed under nitrogen atmosphere with a Perkin Elmer Pyris 1 Thermal Analyzer at a heating rate of 5 °C min^{-1}. The RGO nanosheets used for AFM, UV-Vis spectroscopy and TGA were extracted from the RGO-gelatin hydrogels. A small fraction of hydrogel was smashed and washed three times using distilled water (80 °C), followed by centrifugation (at 8000 rpm) at each time, to remove excess and non-grafted gelatin on the graphene surface. Some sediment was lyophilized for TGA tests. The remaining was re-dispersed in distilled water at 1 mg mL^{-1} by stirring and then sonicating for 5 min. The obtained suspension was centrifuged at a lower speed (2000 rpm) for 20 min to remove large particles. The supernatant was taken for characterization under AFM and UV-Vis spectroscopy.

Rheological measurements

Rheological measurements were performed on an AR2000 Advanced Rheometer (TA Instruments). Oscillatory shear measurements were carried out at 25 °C to determine the storage moduli (G') and loss moduli (G'') of the RGO-gelatin hydrogels over an angular frequency range from 0.1 to 100 rad s^{-1} under a fixed strain of 0.1% (in the linear viscoelastic region pre-determined by dynamic strain sweep tests). All measurements were performed with a parallel-plate geometry (diameter 40 mm) equipped with a solvent trap to avoid evaporation. The gap between two parallel plates was fixed at 2 mm.

Swelling tests

As-prepared hydrogels were punched into discs with the same size (15 mm in diameter and 6 mm thick). The hydrogels were frozen by liquid nitrogen before freeze-drying. The freeze-dried hydrogel samples were then immersed in excess distilled water to obtain equilibrium swelling at room temperature. The samples were weighed at 0.5, 1, 3, 6, 12 and 24 h. The measurements were carried out on three replicate samples. The swelling ratio (SR) of the hydrogel was calculated according to Equation 1:

$$SR = \frac{W_s - W_d}{W_d} \tag{1}$$

where W_s is the weight of the swollen hydrogel at the different time interval and W_d is the weight of the freeze-dried hydrogel before immersion in water.

In vitro Biodegradation

The hydrogel cylinders (RGG10H) with dimensions of 6 mm in height and 15 mm in diameter were placed in 8 mL PBS solution with 0.5 U mL^{-1} collagenase type II and incubated (Shaker Incubator SI500, Stuart) at 37 °C and a speed of 100 rpm for 2, 4, 8, 16, 24 and 32 h. At each time point, the collagenase solution was removed and the remaining hydrogels were washed with distilled water. The hydrogels were then lyophilized at -10 °C after frozen by using liquid nitrogen. The degradation was calculated by dividing the lost weight of the lyophilized samples by the original weight of the untreated lyophilized hydrogels. The sample size was three per group. The control samples underwent degradation in the PBS solution without collagenase.

Results and discussion

The RGO-gelatin hydrogels were synthesized by heating the mixture of an aqueous GO suspension and a gelatin water solution at 95 °C for 24 h. According to the literature,[20, 40] gelatin chains could be grafted onto GO sheets whilst reducing them into RGO. It has been shown that different types of amine can react with some of the functional groups on GO via two main routes, i.e., ring-opening amination of epoxy on the surface of GO and the amidation reaction of carboxylic acid groups at the edges of GO, both with the amino groups of gelatin by thermal treatment.[41-43] The hydrogen bonding between amine and hydroxyl on the GO was also proposed in the previous literature.[44] It is, therefore, hypothesized that the main interactions between GO and gelatin during the hydrogel formation process could be the same as discussed above, though the nature of chemical reactions is not totally clear due to the complexity of the GO structure.[15] These proposed main interactions are illustrated in Scheme 1.[41] Through the chemical and physical interactions between GO and gelatin, GO sheets are expected to cross-link with gelatin chains and form a hydrogel whilst being reduced to RGO.
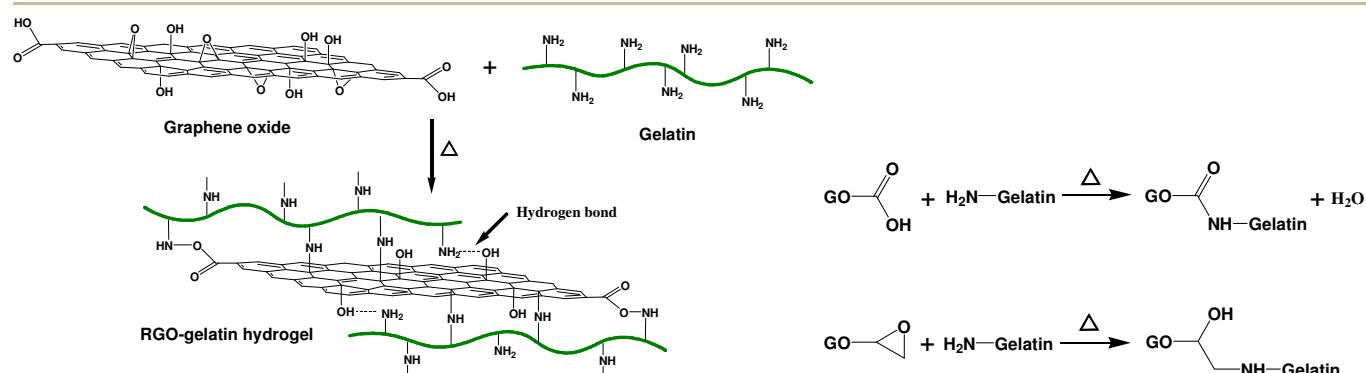
Scheme 1 Illustration of the proposed main chemical reactions and physical interactions between GO nanosheets and gelatin to produce a RGO–gelatin hydrogel.
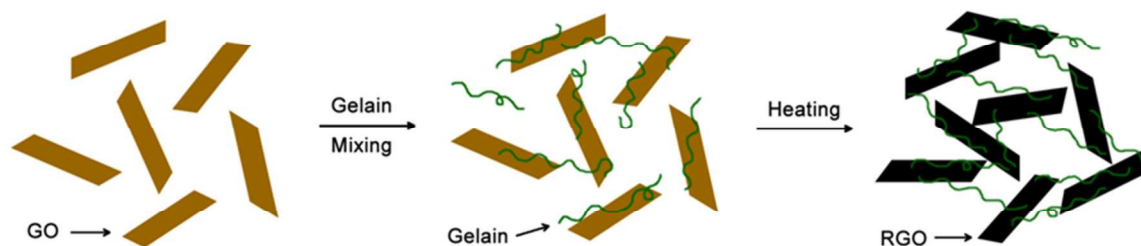
Scheme 2 Illustration of the hydrogel formation process.

In order to verify the above hypotheses, changes to the chemical structure of gelatin and GO during the synthesis were first investigated by FT-IR spectroscopy. Fig. 1A shows FT-IR spectra of graphite, GO, gelatin and lyophilized RGO-gelatin hydrogels with different gelatin contents. The spectrum of the graphite (Curve a) only shows a weak absorbance of O–H stretching at 3400 cm^{-1} caused by the absorbed water. The spectrum of GO (Curve b) reveals the presence of different types of oxygenated functional group: O–H stretching bond at 3200-3400 cm^{-1}, C=O carbonyl stretching at 1729 cm^{-1}, C–OH stretching vibration at 1361 cm^{-1}, C–O–C epoxy at 1225 cm^{-1} and C–O alkoxy at 1046 cm^{-1}, as well as C=C vibrations from aromatic structure domains at 1621 cm^{-1}.[45, 46] The spectrum of gelatin (Curve f) is recorded as a control, and its characteristic groups are identified: amide I vibration (C=O, 1627 cm^{-1}), amide II bending vibration (N–H, 1521 cm^{-1}), amide III (1238 cm^{-1}), and N–H stretching (3262 cm^{-1}).[47] Eliminating the intensity varying due to the various GO weight ratio in the nanocomposites, the epoxy vibration (1225 cm^{-1}) of GO is weakened in RGG5H and RGG10H (Curves d and e) confirming the ring-opening reaction between epoxy groups of GO and amino groups of gelatin.[41] Similarly, the C=O stretching vibration of GO gradually decreases in its intensity as the gelatin content increases and almost disappears in RGG10H. This illustrates the amidation of carboxyl groups at the edge of GO with amino groups of gelatin, which agrees well with the previous report.[42] These FT-IR results confirm the proposed chemical reactions illustrated in Scheme 1.[41] The ring-opening reaction between epoxy groups and amino groups is a nucleophilic substitution reaction resulting in the creation of hydroxyl groups and formation of C–N bonds. The amidation of carboxyl groups of GO with amino groups of gelatin is a condensation reaction which requires heat.

It is also found that the modest vibration C–OH centered at 1361 cm^{-1} and the strong C–O vibration at 1046 cm^{-1} in GO become weaker with an increasing amount of gelatin in the hydrogel, indicating partial elimination of the hydroxyl groups of RGO during the synthesis of the hydrogel.[20, 40] Furthermore, gelatin has residual −NH_2 groups, −NH_3^+ and −COO^- ions on its macromolecular chains and these functional groups can form hydrogen-bonding and electrostatic attractions with the residual hydroxyl and carboxyl groups of RGO as well as with their adjacent gelatin molecules.[43] Thus, the chemical and physical bonds between the RGO sheets and gelatin chains are the driven forces to link the two components together to form a 3D continuous network, i.e. a RGO-gelatin
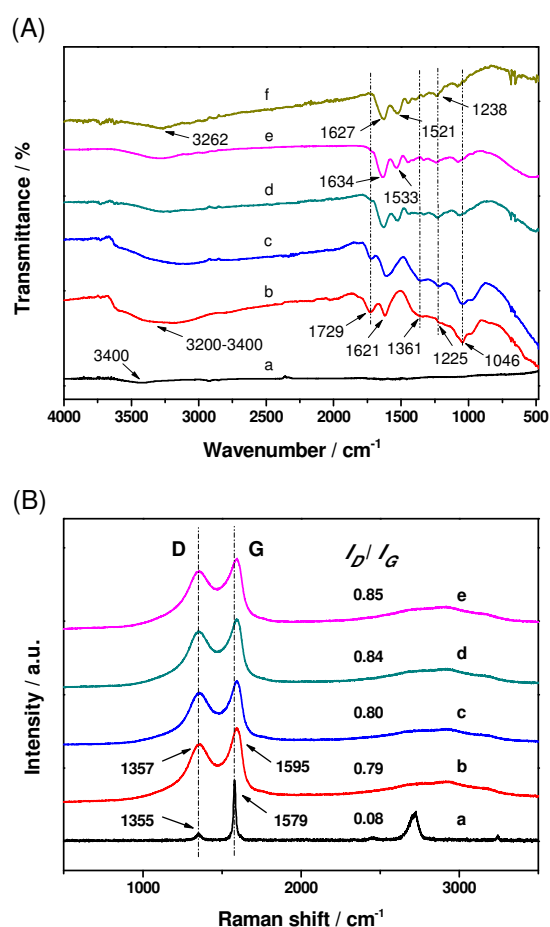

Fig. 1 (A) FT-IR and (B) Raman spectra of (a) graphite, (b) GO, and (c-e) lyophilized RGO-gelatin hydrogels: (c) RGG2H, (d) RGG5H, (e) RGG10H, and (f) gelatin. The ratios of I_D/I_G for the hydrogels are also shown in the figure.

hydrogel, as illustrated in Scheme 2.

The structural changes of graphene materials in the hydrogels could also be identified in Raman spectra, as shown in Fig. 1B. The pristine graphite (Curve a) shows a sharp G band at 1579 cm^{-1} in relation to the in-phase vibration of the graphite lattice, and a weak D band is found at 1355 cm^{-1}, which is induced by structural disorder and defects.[48] After oxidation, the D band becomes
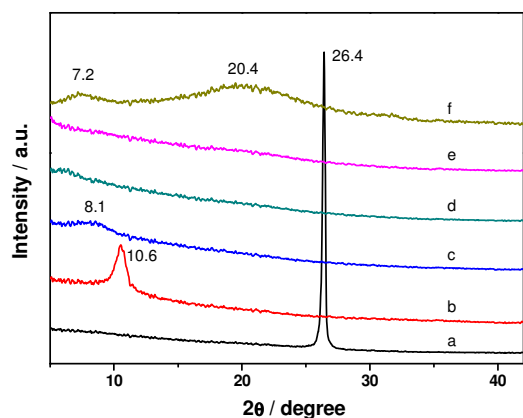
Fig. 2 XRD patterns of (a) graphite, (b) GO, and (c-e) lyophilized RGO-gelatin hydrogels: (c) RGG2H, (d) RGG5H, (e) RGG10H, and (f) gelatin.

stronger and broader in GO (Curve b). As a result, the intensity ratio of D band to G band, I_D/I_G (0.79), increases significantly compared to that of graphite (0.08), which is associated with a marked decrease in the graphite crystal size arising from a considerably higher level of disorder of the graphene structure and increased defects.[49, 50] The G band becomes slightly asymmetric in GO due to its overlap with the defect-related G' band at 1620 cm^{-1}.[49] As depicted in Fig. 1B, the lyophilized RGO-gelatin hydrogels (Curves c-e) have similar profiles to that of GO. With the increase of gelatin content in the RGO hydrogels, the intensity ratio of I_D/I_G increases slightly from 0.79 to 0.85. This variation is lower compared to the values found for the reduction of GO by other chemicals reported in the literature,[51, 52] which may be due to the partial reduction of GO as described subsequently and hence only a small change to the graphite crystal size.

XRD patterns of graphite, graphite oxide, gelatin and the lyophilized RGO-gelatin hydrogels are shown in Fig. 2. Graphite (Curve a) shows a sharp and strong peak at 26.4°, corresponding to a typical interlayer spacing (d) of 0.34 nm.[53] Gelatin powder typically exhibits two broad peaks centered at 20.4° and 7.2°, due to the crystalline structure originated from a-helix and triple-helical structure.[54] A slightly broader 2θ peak for GO (Curve b) appears at 10.6°, corresponding to an interlayer spacing of 0.83 nm. A weak broad peak centered at 8.1° (d = 1.09 nm) is observed for the freeze-dried RGG2H with the least gelatin content (16.7 wt.%). The presence of this weak peak suggests there are a small amount of stacks of not fully dispersed RGO sheets in the hydrogel presumably due to the insufficient gelatin content. In contrast, there is no observable diffraction peak for the lyophilized RGG10H which comprises the highest gelatin content (50.0 wt.%) (Curve d), indicating that graphite and gelatin have completely lost their order in the crystal structure and RGO nanosheets are dispersed in the hydrogel as exfoliated single nanosheets.[55]

The morphology of GO and RGO nanosheets is illustrated in Fig. 3A. AFM results show that the thickness of a single layer of
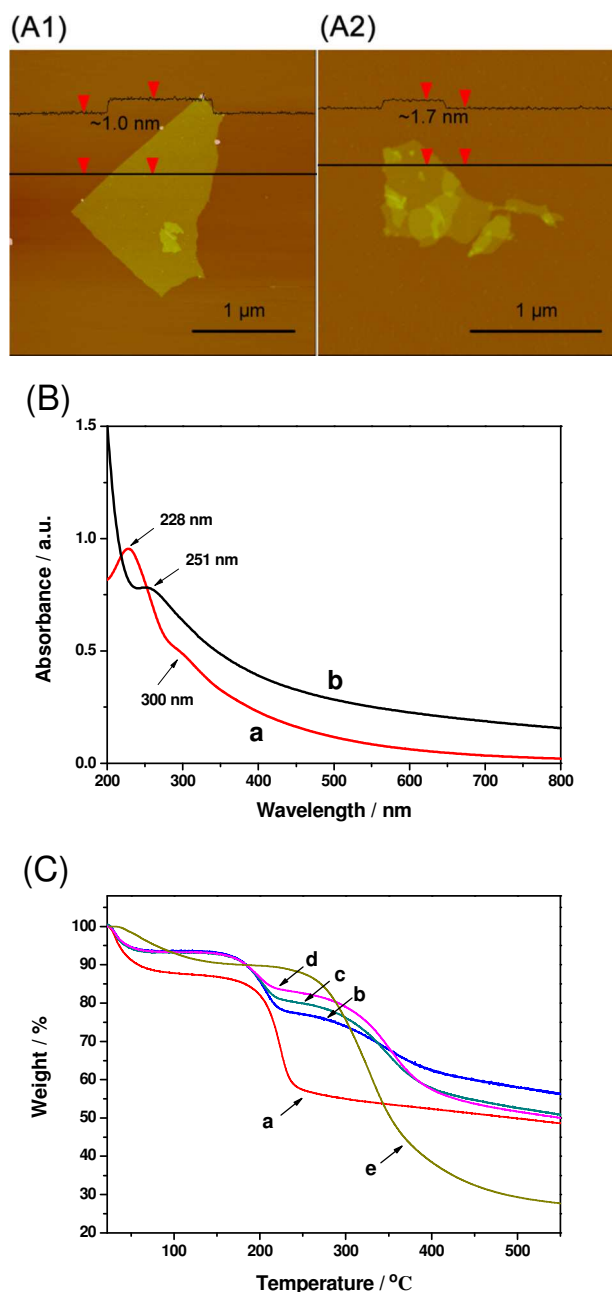

Fig. 3 Tapping mode AFM topographic images of (A1) single-layer nanosheets of GO and (A2) RGO extracted from RGG10H with the height profile. (B) UV-Vis absorption spectra of (a) GO and (b) RGO (extracted from RGO-gelatin hydrogel, RGG10H) aqueous suspension at a concentration of 0.1 mg mL^{-1}. (C) TGA curves of (a) GO, (b-d) RGO (extracted from corresponding RGG2H, RGG5H and RGG10H, respectively), and (e) gelatin.

GO is ~1.0 nm (Fig. 3(A1)), whereas the thickness of RGO increases to ~1.7 nm (Fig. 3(A2)), confirming the grafting of gelatin molecules on the surface of GO. The thickness of the GO determined by AFM is slightly higher than that from XRD, due to the presence of a water layer between GO and the substrate and perhaps also to the resolution of the AFM tip.[56] The lateral sizes of the GO and RGO sheets are both typically in the range of several hundreds of nanometers to a few micrometers, implicating that the synthesis
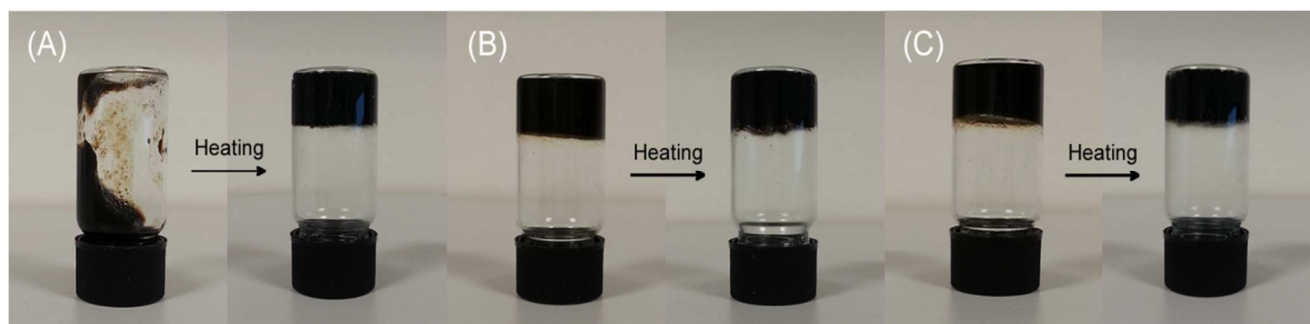
Fig. 4 Illustration of the evolution of the formation of the hydrogels: (A) RGG2H, (B) RGG5H and (C) RGG10H before and after heat treatment during the hydrogel synthesis. Diameter of the containers: 15 mm.

process did not reduce the size. RGO sheets extracted from the RGO-gelatin hydrogel were characterized by UV-Vis spectroscopy. The absorption spectra confirmed the chemical reduction of GO to RGO during the hydrogel formation under the heat treatment (Fig. 3B). The spectrum of GO shows a absorption peak at 228 nm referring to $\pi \rightarrow \pi^*$ transitions of aromatic C=C bonds and a shoulder at 300 nm ascribed to $n \rightarrow \pi^*$ transitions of C=O bonds.[57, 58] In contrast, the peak at 228 nm in the spectrum of RGO shifts to 251 nm, indicating the electronic conjugation is restored.[57] This shift is smaller than that (to 270 nm) of hydrazine reduced GO,[59] and that (266 nm) of GO nanosheets reduced in a gelatin solution with an excessive amount of gelatin at 95 °C for 24 h.[20] It indicates a partial restoration of the sp^2 carbon network of RGO in this work, i.e., partial reduction of GO as previously discussed, even at the largest gelatin content used. The disappearance of the peak at 300 nm corresponds to de-oxygenation of the C=O groups of GO nanosheets.[60]

TGA was used to determine the composition of the RGO sheets extracted from the RGO-gelatin hydrogels, and the results are shown in Fig. 3C. The weight losses below 100 °C are all considered due to the evaporation of absorbed water. The TGA curve of GO shows its major weight loss (~43 wt.%) at around 210 °C, attributed to pyrolysis of the oxygen-containing functional groups generate CO, CO2 and steam.[61] As the temperature is further increased, it shows a very slow change in the weight. Gelatin shows a major weight loss (~59 wt.%) in the region from 250 °C to 500 °C. The TGA curves of all the three RGOs can be divided to two major stages in terms of weight loss. The first occurs between 100 °C and 250 °C, and the second appears from 250 to 550 °C. One can deduce that the first loss is mainly attributed to the pyrolysis of the functional groups on the GO while the latter is mainly due to the pyrolysis of the gelatin chains grafted on the RGO sheets. The RGO extracted from the hydrogel with a higher gelatin content exhibits a less weight loss (RGG10 < RGG5H < RGG2H) from 100 °C to 250 °C, in coordination to the pyrolysis of the relatively lower content of GO. In reverse, the corresponding RGO has a higher weight loss (RGG10 > RGG5H > RGG2H) in the range of 250–550 °C, in accordance with the pyrolysis of the gelatin. The weight percentages of gelatin molecules grafted on the RGO sheets were calculated after the elimination of the absorbed water, which are 34.7, 48.2 and

54.1 wt.% for the hybrid nanosheets extracted from RGG2H, RGG5H and RGG10H, respectively. This further clarifies that a fraction of gelatin in the hydrogel covalently bonded to the graphene nanosheets and the rest interacted with each other and RGO through physical bonding.

Fig. 4 demonstrates that the evolution of the form of the RGO-gelatin hydrogels before and after heat treatment during the hydrogel synthesis. A precursor of RGG2H, a mixture of GO and gelatin suspension (Fig. 4A), remains as a sol before heating. In contrast, the precursors of RGG5H and RGG10H are hydrogels (Fig. 4B and 4C) after physically mixing the two components (confirmed by the tube inversion method), in which the physically bonding is strong enough to form the hydrogel due to the appropriate gelatin content.[34] After heat treatment, the three RGO-gelatin hydrogels are obtained. Their black color is also evidence of the reduction of GO in the hydrogel compared with dark brown color of their GO precursors. For all the three hydrogel precursors, chemical reactions occurred between abundant NH_2 groups on gelatin chains and carboxyl and epoxy groups on the GO nanosheets during the heating process (illustrated in Scheme 1), leading to the reduction of GO. In RGG2H, this also results in the formation of a stable 3D network. All the three RGO-gelatin hydrogels are formed by RGO sheets connecting the adjacent gelatin chains by the covalent bonds and hydrogen bonding as depicted in Scheme 2.

Fig. 5A shows the rheological properties of RGGHs with different gelatin contents. The RGO-gelatin hydrogels exhibit typical rheological behavior of hydrogels. The storage modulus is nearly frequency independent, showing only slight increase as the angular frequency increases. The loss factor Tanδ is also relatively independent to the angular frequency in the testing range (Fig. 5B). The storage moduli are one order of magnitude greater than the corresponding loss moduli, indicating the hydrogels are stable networks and more elastic than viscous.[30] The storage moduli of the RGGHs increase as the content of gelatin increases, while remaining a similar water content (~98.0–98.8 wt.%). The storage modulus of RGG10H is 172.3 kPa at 10 rad s^{-1}, which is 89% greater than 91.1 kPa of RGG5H and 169% greater than 64.4 kPa of RGG2H, respectively. The more gelatin is introduced to the system, the more chemical cross-linking sites between the gelatin chains and GO nanosheets are created, leading to a more stable network and less mobility of the macromolecular chains. Previously, we reported that physically cross-linked GO-gelatin hydrogels had storage
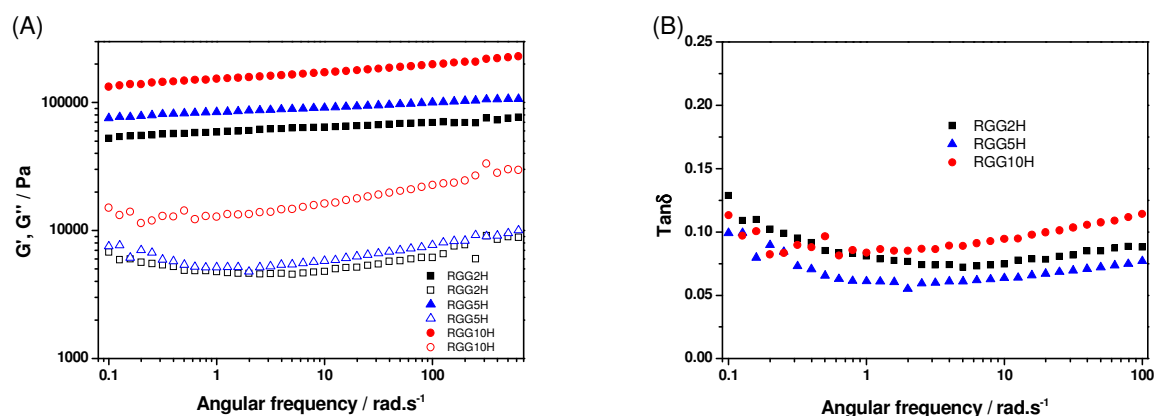
Fig. 5 (A) Storage moduli G' (solid) and loss moduli G'' (hollow), and (B) loss factor Tanδ of lyophilized hydrogels.

moduli of 114.5 kPa and 3.2 kPa with the same composition of RGG10H and RGG5H, respectively. The storage modulus of RGG10H is 50% higher than that of its physically cross-linked counterpart hydrogel, while the value of RGG5H is 27-fold higher than that of its GO counterpart. The results indicate the covalent bonds considerably enhance the mechanical performance of the RGGHs compared to the physically cross-linked counterpart hydrogels, in particular those weaker hydrogels with a lower gelatin concentration.

The rheological data are also used to determine the cross-linking density, N, and the number average molecular weight of polymer chains between the cross-linkers in the hydrogel, $\overline{M}_c$. N is defined as the number of active polymer chains per unit volume in the network. The cross-linking density is determined by using the rubber elasticity theory, which is presented in Equation 2 below.[62]

$$G = NkT = \frac{cRT}{\overline{M}_c}\left(1 - \frac{2\overline{M}_c}{\overline{M}}\right) \tag{2}$$

in which c is the concentration of the polymer in the hydrogel, R is the gas constant (8.31 m^3 Pa K^{-1} moL^{-1}), k is Boltzmann constant (1.38065 × 10^{-23} J K^{-1}), T is absolute temperature (298 K), $\overline{M}$ is the average molecular weight of the polymer, and G is the static shear modulus. According to the literature,[63] a correlation between static Young's modulus and dynamic Young's modulus can be empirically established, which can then be converted to the relationship between the static shear modulus G and dynamic shear modulus

G' (Equation 3).[34, 64]

$$G = 0.629G' - \frac{1.586}{2(1+v)} \tag{3}$$

where v is Poisson's ratio. Because the hydrogels are assumed as ideal rubbers, v is taken as 0.5.[65] By applying the experimental values of G' to Equations 2 and 3, the results are determined and shown in Table 1.

For the hydrogels with a fixed graphene content, N increases from 99×10^{23} m^{-3} for RGG2H to 139×10^{23} m^{-3} for RGG5H and 263×10^{23} m^{-3} for RGG10H. Correspondingly, $\overline{M}_c$ between the neighboring cross-linking sites (RGO nanosheets) increases from 122 to 214 and 226 g moL^{-1}. There is a high quantity of covalent and non-covalent cross-linking sites for the formation of the RGO-gelatin hydrogel, due to the abundant functional groups from both GO sheets and gelatin chains. This gives rise to the relatively high values of N and relatively low values of $\overline{M}_c$ presented in Table 1. As one would expect, a higher cross-linking density leads to a stiffer hydrogel. The mechanical properties of the hydrogels could be modulated by varying the composition and hence controlling the cross-linking density, similar to our previous observation for GO-gelatin nanocomposite hydrogels.[34]

Fig. 6 shows the morphology of a lyophilized GO suspension and RGO-gelatin hydrogels under SEM. The RGGHs consist of the same concentration of GO in water as the neat GO suspension, regardless

Table 1 Cross-linking densities and number average molecular weights of polymer chains between the adjacent cross-linking sites in the RGO-gelatin hydrogels with varying compositions.

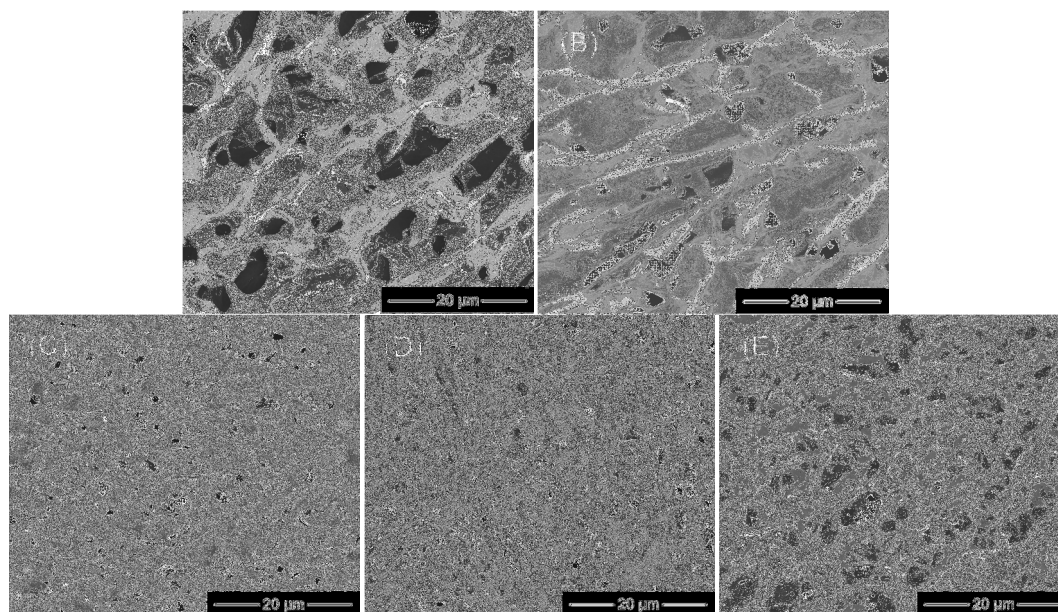| Sample	Gelatin (mg mL^{-1})	GO (mg mL^{-1})	Storage Modulus, G' (kPa)	Cross-linking Density, N (×10^{23} m^{-3})	Number Average Molecular Weight, $\overline{M}_c$ (g moL^{-1})
RGG2H	2	10	64.4	99	122
RGG5H	5	10	91.1	139	214
RGG10H	10	10	172.3	263	226

Fig. 6 SEM images of cross-section surfaces of (A) lyophilized GO suspension (10 mg mL^{-1}), (B) lyophilized precursor mixture of RGG2H before gelation (containing 10 mg mL^{-1} GO and 2 mg mL^{-1} gelatin), (C) lyophilized RGG2H, (D) RGG5H, and (E) RGG10H.

the difference in gelatin content. All the lyophilized samples show porous structure despite of the broad variation in the pore size. The porous structure of the lyophilized GO suspension (Fig. 6A) was formed due to the structural changes during the drying stage; the GO sheets contact to each other to form the network presumably facilitated by the hydrogen bonding between GO sheets and the residual hydrogen-bonded water molecules between GO sheets.[66] Fig 6B shows a lyophilized GO-gelatin suspension, a precursor of RGG2H prior to the gelation process. It has a similar porous structure to the lyophilized GO suspension although the additional gelatin also contributes to the formation of hydrogen bonds in addition to water molecules. In contrast, the lyophilized RGG2H (Fig. 6C) possesses much smaller pores, with an average pore size of 2.3 (±1.1) μm. This is because when the hydrogel is formed GO sheets cross-link with gelatin chains to form a much finer network structure, and the stable network within the hydrogels restricts the growth of ice crystals during the freezing process.[67] RGG5H has a slightly lower average pore size (1.7±0.7 μm) to RGG2H, whereas the value of RGG10H is significantly greater (3.2±1.2 μm). The average pore sizes of RGG5H and RGG10H are much smaller than those (6.2±4.5 μm and 7.7±5.4 μm, respectively) of physically cross-linked GO-gelatin nanocomposite hydrogels with the same composition reported in our previous work.[34] This may be due to reconstruction of the microstructure of RGO-gelatin nanocomposite triggered by the movement of graphene sheets and gelatin chains during the heating process, though there is no notable volume change before and after hydrogel formation. The finer structure also contributes to the superior mechanical performance of the RGO-gelatin nanocomposite hydrogels as opposed to those of the GO-gelatin nanocomposite hydrogels as previously discussed.

Since the hydrogel RGG10H has the highest storage modulus in the current study, it is used for subsequent investigation of the swelling and degradation behavior. Fig. 7A shows the water swelling
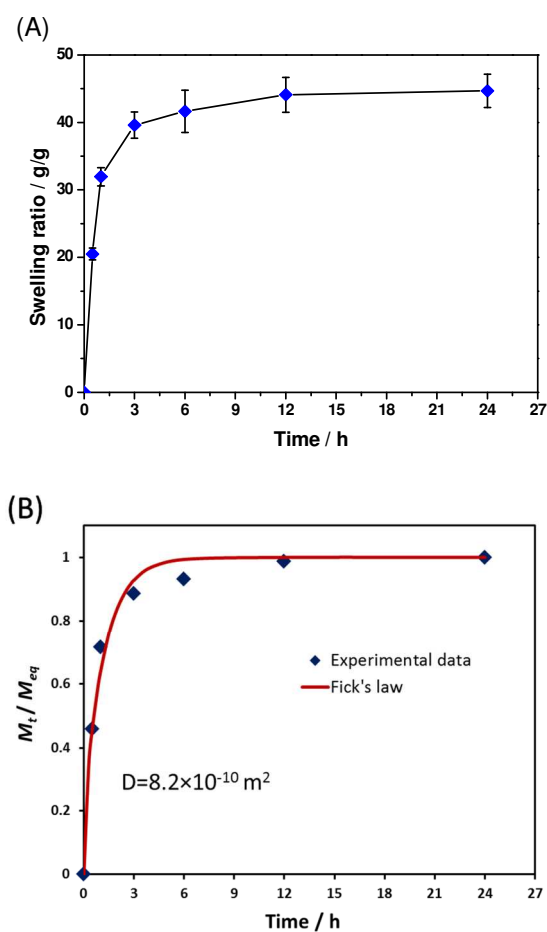

Fig. 7 (A) Swelling behavior of a RGO-gelatin hydrogel (RGG10H), and (B) M_t/M_{eq} as a function of time t for RGG10H.
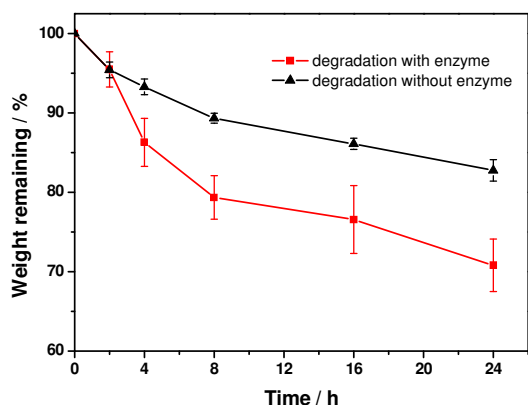
Fig. 8 Degradation profiles of the same hydrogel with and without collagenase in PBS solution.

behavior of the lyophilized hydrogel (RGG10H). The swelling curve is steep at the initial state and then turns to a plateau. It reaches equilibrium by 24 h at a swelling weight ratio of 44.7. Fick's law (Equation 4)[68] was used to describe water swelling behavior of the RGO-gelatin hydrogel.

$$M_t/M_{eq} = 1 - (8/\pi^2)\sum_{m=0}^{\infty} \frac{exp[-\pi^2(2m+1)^2 Dt/L^2]}{(2m+1)^2} \qquad (4)$$

where M_t is the swelling degree at time t, M_{eq} is the equilibrium swelling degree, D is the diffusion coefficient of water molecules, and L is the thickness of the specimens. The diffusion coefficient, D, derived from Equation 4, is 8.2×10^{-10} m^2 s^{-1}. It can be seen from Fig. 7B that the theoretical values fit the experimental data very well. Thus, one can predict the swelling behavior of the RGO-gelatin hydrogels by using the Fick's law.

Fig. 8 shows the degradation profiles of the hydrogel RGG10H at body temperature in the PBS solutions with and without the presence of collagenase. In the initial 2 h, the sample undergoes almost the same degradation rate with and without the enzyme, which can be interpreted as weight loss of the loose gelatin molecules due to diffusion. Afterwards, there is a much more considerable weight loss of the hydrogel with collagenase than that without the enzyme. After 24 h, 29% of the original weight lost in the collagenase degradation, which is 70% higher than the value (17%) obtained without enzyme. These results also show that the RGO-gelatin hydrogel is more stable than GO-gelatin methacrylate hydrogels with only 30% weight[37] remaining after the same period of time. This can be ascribed to the higher cross-linking density in the former. Since the collagenase attacks peptide linkages[37], the main weight loss is mainly due to the degradation of gelatin molecules although there might be a small amount of RGO sheets detached from the bulk hydrogel.

Conclusions

RGO-gelatin nanocomposite hydrogels were synthesized by heating the mixture of a GO suspension and a gelatin solution at various weight ratios at 95 °C for 24 h, without using a chemical cross-linker. GO acted as a multi-functional cross-linker to connect the surrounding gelatin chains to form a 3D network, while gelatin acted simultaneously as a reducing agent and a biocompatibilizer for GO, as well as a building component of the hydrogel. The chemical (mainly) and physical cross-linking between graphene sheets and gelatin chains within the hydrogel was confirmed by FT-IR, Raman spectroscopy, AFM, TGA and UV-Vis spectroscopy. SEM image revealed the internal porous morphology of the hydrogels. The storage modulus of the hydrogel was tuneable by changing the gelatin concentration in the precursor mixture. With the concentration of gelatin of 10 mg mL^{-1} and the water content of 98 wt.%, the highest storage modulus of RGO-gelatin hydrogels was 172.3 kPa, 50% higher than that[34] of its physical cross-linked counterpart. The freeze-dried hydrogel reached equilibrium in 24 h at a swelling weight ratio of 44.7, and the water swelling behavior follows Fick's diffusion law. The hydrogels demonstrated an enzyme-favorite degradation with 71% weight remained after degradation with collagenase for 24 h. The biodegradable RGO-gelatin hydrogels could have potential in tissue engineering and drug delivery.

Notes and references

1   K. Deligkaris, T. S. Tadele, W. Olthuis and A. van den Berg, *Sens. Actuat. B,* 2010, **147**, 765-774.
2   K. Kabiri, H. Omidian, M. J. Zohuriaan-Mehr and S. Doroudiani, *Polym. Compos.,* 2011, **32**, 277-289.
3   A. S. Hoffman, *Adv. Drug Delivery Rev.,* 2002, **54**, 3-12.
4   K. Y. Lee and D. J. Mooney, *Chem. Rev.,* 2001, **101**, 1869-1880.
5   N. A. Peppas, J. Z. Hilt, A. Khademhosseini and R. Langer, *Adv. Mater.*, 2006, **18**, 1345-1360.
6   K. Haraguchi and T. Takehisa, *Adv. Mater.*, 2002, **14**, 1120-1124.
7   Z. Hu and G. Chen, *J. Mater. Chem. A*, 2014, **2**, 13593-13601.
8   K. S. Novoselov, A. K. Geim, S. V. Morozov, D. Jiang, Y. Zhang, S. V. Dubonos, I. V. Grigorieva and A. A. Firsov, *Science*, 2004, **306**, 666-669.
9   A. K. Geim and K. S. Novoselov, *Nat. Mater.*, 2007, **6**, 183-191.
10 C. Soldano, A. Mahmood and E. Dujardin, *Carbon*, 2010, **48**, 2127-2150.
11 O. C. Compton and S. T. Nguyen, *Small*, 2010, **6**, 711-723.
12 C. Chung, Y.-K. Kim, D. Shin, S.-R. Ryoo, B. H. Hong and D.-H. Min, *Acc. Chem. Res.*, 2013, **46**, 2211-2224.
13 P. Wei, W. Bao, Y. Pu, C. N. Lau and J. Shi, *Phys. Rev. Lett.*, 2009, **102**, 166808 (1-4).
14 J. Zhu, M. Chen, Q. He, L. Shao, S. Wei and Z. Guo, *RSC Adv.*, 2013, **3**, 22790-22824.
15 D. R. Dreyer, S. Park, C. W. Bielawski and R. S. Ruoff, *Chem. Soc. Rev.*, 2010, **39**, 228-240.
16 S. Mao, H. Pu and J. Chen, *RSC Adv.,* 2012, **2**, 2643-2662.
17 O. N. Ruiz, K. S. Fernando, B. Wang, N. A. Brown, P. G. Luo, N. D. McNamara, M. Vangsness, Y.-P. Sun and C. E. Bunker, *ACS Nano*, 2011, **5**, 8100-8107.

18 X. Zhang, J. Yin, C. Peng, W. Hu, Z. Zhu, W. Li, C. Fan and Q. Huang, *Carbon*, 2011, **49**, 986-995.

19 J. Kim, Y.-R. Kim, Y. Kim, K. T. Lim, H. Seonwoo, S. Park, S.-P. Cho, B. H. Hong, P.-H. Choung and T. D. Chung, *J. Mater. Chem. B*, 2013, **1**, 933-938.

20 K. P. Liu, J. J. Zhang, F. F. Cheng, T. T. Zheng, C. M. Wang and J. J. Zhu, *J. Mater. Chem.*, 2011, **21**, 12034-12040.

21 K. Yang, J. Wan, S. Zhang, Y. Zhang, S.-T. Lee and Z. Liu, *ACS Nano*, 2010, **5**, 516-522.

22 K. Yang, H. Gong, X. Shi, J. Wan, Y. Zhang and Z. Liu, *Biomaterials*, 2013, **34**, 2787-2795.

23 C. C. Huang, H. Bai, C. Li and G. Q. Shi, *Chem. Commun.*, 2011, **47**, 4962-4964.

24 Y. X. Xu, K. X. Sheng, C. Li and G. Q. Shi, *ACS Nano*, 2010, **4**, 4324-4330.

25 Y. Xu, X. Huang, Z. Lin, X. Zhong, Y. Huang and X. Duan, *Nano Res.*, 2013, **6**, 65-76.

26 H. Wang, H. Yi, X. Chen and X. Wang, *J. Mater. Chem. A*, 2014, **2**, 1165-1173.

27 S. Das, F. Irin, L. Ma, S. K. Bhattacharia, R. C. Hedden and M. J. Green, *ACS Appl. Mater. Interf.*, 2013, **5**, 8633-8640.

28 C. Hou, Y. Duan, Q. Zhang, H. Wang and Y. Li, *J. Mater. Chem.*, 2012, **22**, 14991-14996.

29 H. Zhou, W. Yao, G. Li, J. Wang and Y. Lu, *Carbon*, 2013, **59**, 495-502.

30 B. Adhikari and A. Banerjee, *Soft Matter*, 2011, **7**, 9259-9266.

31 Y. Wang, P. Zhang, C. F. Liu and C. Z. Huang, *RSC Adv.*, 2013, **3**, 9240-9246.

32 Y. Tabata and Y. Ikada, *Adv. Drug Delivery Rev.*, 1998, **31**, 287-301.

33 S. Young, M. Wong, Y. Tabata and A. G. Mikos, *J. Control. Release,* 2005, **109**, 256-274.

34 Y. Piao and B. Chen, *J. Polym. Sci. B,* 2014, **53**, 356-367.

35 S. Faghihi, A. Karimi, M. Jamadi, R. Imani and R. Salarian, *Mater. Sci. Eng., C,* 2014, **38**, 299-305.

36 S. Faghihi, M. Gheysour, A. Karimi and R. Salarian, *J. Appl. Phys.,* 2014, **115**, 083513 (1-6).

37 S. R. Shin, B. Aghaei-Ghareh-Bolagh, T. T. Dang, S. N. Topkaya, X. Gao, S. Y. Yang, S. M. Jung, J. H. Oh, M. R. Dokmeci and X. S. Tang, *Adv. Mater.*, 2013, **25**, 6385-6391.

38 W. S. Hummers and R. E. Offeman, *J. Am. Chem. Soc.*, 1958, **80**, 1339-1339.

39 D. C. Marcano, D. V. Kosynkin, J. M. Berlin, A. Sinitskii, Z. Z. Sun, A. Slesarev, L. B. Alemany, W. Lu and J. M. Tour, *ACS Nano*, 2010, **4**, 4806-4814.

40 J. An, Y. Gou, C. Yang, F. Hu and C. Wang, *Mater. Sci. Eng. C,* 2013, **33**, 2827-2837.

41 O. C. Compton, D. A. Dikin, K. W. Putz, L. C. Brinson and S. T. Nguyen, *Adv. Mater.*, 2010, **22**, 892-896.

42 J. S. Chung, E. J. Kim and S. H. Hur, *Chem. Eng. J.,* 2014, **246**, 64-70.

43 A. B. Bourlinos, D. Gournis, D. Petridis, T. Szabó, A. Szeri and I. Dékány, *Langmuir*, 2003, **19**, 6050-6055.

44 Y. Matsuo, T. Miyabe, T. Fukutsuka and Y. Sugie, *Carbon*, 2007, **45**, 1005-1012.

45 Y.-P. Zhang, J.-J. Xu, Z.-H. Sun, C.-Z. Li and C.-X. Pan, *Prog. Nat. Sci.*, 2011, **21**, 467-471.

46 T. Yang, L.-H. Liu, J.-W. Liu, M.-L. Chen and J.-H. Wang, *J. Mater. Chem.*, 2012, **22**, 21909-21916.

47 C. Yang, L. Xu, Y. Zhou, X. Zhang, X. Huang, M. Wang, Y. Han, M. Zhai, S. Wei and J. Li, *Carbohydr. Polym.,* 2010, **82**, 1297-1305.

48 F. Tuinstra and J. L. Koenig, *J. Chem. Phys.*, 1970, **53**, 1126-1130.

49 K. N. Kudin, B. Ozbas, H. C. Schniepp, R. K. Prud'Homme, I. A. Aksay and R. Car, *Nano Lett.*, 2008, **8**, 36-41.

50 K. Sato, R. Saito, Y. Oyama, J. Jiang, L. Cançado, M. Pimenta, A. Jorio, G. G. Samsonidze, G. Dresselhaus and M. Dresselhaus, *Chem. Phys. Lett.*, 2006, **427**, 117-121.

51 K.-X. Sheng, Y.-X. Xu, C. Li and G.-Q. Shi, *New Carbon Mater.*, 2011, **26**, 9-15.

52 S. Stankovich, D. A. Dikin, R. D. Piner, K. A. Kohlhaas, A. Kleinhammes, Y. Jia, Y. Wu, S. T. Nguyen and R. S. Ruoff, *Carbon*, 2007, **45**, 1558-1565.

53 H.-K. Jeong, H.-J. Noh, J.-Y. Kim, M. Jin, C. Park and Y. Lee, *Europhys. Lett.,* 2008, **82**, 67004 (1-5).

54 A. Bigi, S. Panzavolta and K. Rubini, *Biomaterials*, 2004, **25**, 5675-5680.

55 K. Haraguchi, H. J. Li, K. Matsuda, T. Takehisa and E. Elliott, *Macromolecules*, 2005, **38**, 3482-3490.

56 M. J. McAllister, J.-L. Li, D. H. Adamson, H. C. Schniepp, A. A. Abdala, J. Liu, M. Herrera-Alonso, D. L. Milius, R. Car and R. K. Prud'homme, *Chem. Mater.*, 2007, **19**, 4396-4404.

57 E.-Y. Choi, T. H. Han, J. Hong, J. E. Kim, S. H. Lee, H. W. Kim and S. O. Kim, *J. Mater. Chem.*, 2010, **20**, 1907-1912.

58 D. Zhang, X. Liu and X. Wang, *J. Inorg. Biochem.*, 2011, **105**, 1181-1186.

59 D. Li, M. B. Muller, S. Gilje, R. B. Kaner and G. G. Wallace, *Nat. Nanotechnol.*, 2008, **3**, 101-105.

60 G. Eda, J. Ball, C. Mattevi, M. Acik, L. Artiglia, G. Granozzi, Y. Chabal, T. D. Anthopoulos and M. Chhowalla, *J. Mater. Chem.*, 2011, **21**, 11217-11223.

61 R. Larciprete, P. Lacovig, S. Gardonio, A. Baraldi and S. Lizzit, *J. Phys. Chem. C*, 2012, **116**, 9900-9908.

62 L. R. G. Treloar, *The Physics of Rubber Elasticity*, Clarendon Press, Oxford, 1975, pp. 1-2, 160-170.

63 J. Sabbagh, J. Vreven and G. Leloup, *Dent. Mater.*, 2002, **18**, 64-71.

64 T. K. L. Meyvis, B. G. Stubbe, M. J. Van Steenbergen, W. E. Hennink, S. C. De Smedt and J. Demeester, *Int. J. Pharm.*, 2002, **244**, 163-168.

65 C. Macosko, *Rheology: Principles, Measurements, and Applications*, Wiley-VCH Publishers, New York, 1994, pp. 37-45.

66 D. A. Dikin, S. Stankovich, E. J. Zimney, R. D. Piner, G. H. Dommett, G. Evmenenko, S. T. Nguyen and R. S. Ruoff, *Nature*, 2007, **448**, 457-460.

67 N. Zhang, R. Li, L. Zhang, H. Chen, W. Wang, Y. Liu, T. Wu, X. Wang, W. Wang, Y. Li, Y. Zhao and J. Gao, *Soft Matter*, 2011, **7**, 7231-7239.

68 J. Crank, *The mathematics of diffusion*, Clarendon Press, Oxford, 2nd ed., 1975, 44-62.